

## Relationship between polar cap patches and field-aligned irregularities as observed with an all-sky airglow imager at Resolute Bay and the PolarDARN radar at Rankin Inlet

K. Hosokawa,<sup>1</sup> K. Shiokawa,<sup>2</sup> Y. Otsuka,<sup>2</sup> T. Ogawa,<sup>3</sup> J.-P. St-Maurice,<sup>4</sup> G. J. Sofko,<sup>4</sup> and D. A. Andre<sup>4</sup>

Received 28 August 2008; revised 2 December 2008; accepted 13 January 2009; published 19 March 2009.

[1] Simultaneous two-dimensional observations of airglow enhancement and radar backscatter from field-aligned irregularities (FAIs) associated with polar cap patches were conducted. The spatial structure of 630 nm airglow from polar cap patches was imaged using an all-sky airglow imager at Resolute Bay, Canada, while backscatter echoes from decameter-scale FAIs were observed using the newly constructed HF Polar Dual Auroral Radar Network (PolarDARN) radar at Rankin Inlet, Canada. Both the airglow enhancement and the radar backscatter appeared within a structured region with the spatial extent of about 500–1000 km. The decameter-scale FAIs were found to extend over the entire region of airglow enhancement associated with polar cap patches, indicating that the polar patch plasma became almost fully structured soon after initiation (within approximately 20–25 min). These findings imply that some rapid structuring process of the entire patch area is involved in addition to the primary gradient-drift instabilities.

**Citation:** Hosokawa, K., K. Shiokawa, Y. Otsuka, T. Ogawa, J.-P. St-Maurice, G. J. Sofko, and D. A. Andre (2009), Relationship between polar cap patches and field-aligned irregularities as observed with an all-sky airglow imager at Resolute Bay and the PolarDARN radar at Rankin Inlet, *J. Geophys. Res.*, *114*, A03306, doi:10.1029/2008JA013707.

### 1. Introduction

[2] Polar cap patches, regions of ionospheric plasma density enhancement in the polar cap, are generally generated in the vicinity of the dayside cusp when the IMF is directed southward, and are transported toward the nightside across the polar cap along the streamline of antisunward convection [Crowley, 1996]. A case study has been presented in which patches are formed during northward IMF inside a lobe cell and owing to soft particle precipitation [Oksavik *et al.*, 2006]. However, such patches could not be observed deep inside the polar cap since the transportation due to the antisunward convection is limited when the IMF is directed northward. The dynamics of polar patches have been investigated using a range of ground-based techniques, including all-sky airglow imaging [Weber *et al.*, 1986], coherent HF radar [Ogawa *et al.*, 1998; Milan *et al.*, 2002], incoherent scatter radar [Pedersen *et al.*, 1998, 2000], and ionosonde [MacDougall and Jayachandran, 2007]. The recent development of all-sky

imagers with cooled CCD detectors has made it possible to visualize the two-dimensional structure of polar patches with improved spatial and temporal resolution [e.g., Hosokawa *et al.*, 2006].

[3] Small-scale plasma density irregularities embedded within polar patches, whose scale size ranges from a few tens of kilometers to tens of meters, have been reported by a number of authors [e.g., Weber *et al.*, 1986]. However, the two-dimensional nature of such irregularities has yet to be clarified in detail because most of the past publications employed satellite data [Basu *et al.*, 1994; Kivanc and Heelis, 1997] or incoherent scatter radar data [Pedersen *et al.*, 1998, 2000] to characterize the density irregularities.

[4] The establishment of the Super Dual Auroral Radar Network (SuperDARN) [Greenwald *et al.*, 1995; Chisham *et al.*, 2007] has made it possible to observe radar echoes caused by Bragg scatter from field-aligned irregularities (FAIs) associated with polar patches [Rodger *et al.*, 1994; Ogawa *et al.*, 1998; Milan *et al.*, 2002, 2005]. If such FAIs are generated by gradient-drift instability (GDI), the fastest growth rate at the linear stage is obtained on the trailing edge of patches although the instability can occur everywhere along the boundary of patches, except where the background plasma convection and the electron density gradient are exactly antiparallel [Keskinen and Ossakow, 1982]. Milan *et al.* [2002] reported stronger backscatter power on the trailing edge of radar patches observed by the SuperDARN Finland radar in the vicinity of the dayside cusp. By contrast, on the basis of an examination of nighttime FAIs possibly associated with polar patches, Ogawa *et al.* [1998] demonstrated

<sup>1</sup>Department of Information and Communication Engineering, University of Electro-Communications, Chofu, Japan.

<sup>2</sup>Solar-Terrestrial Environment Laboratory, Nagoya University, Nagoya, Japan.

<sup>3</sup>National Institute of Information and Communications Technology, Koganei, Japan.

<sup>4</sup>Institute for Space and Atmospheric Studies, Department of Physics and Engineering Physics, University of Saskatchewan, Saskatoon, Saskatchewan, Canada.

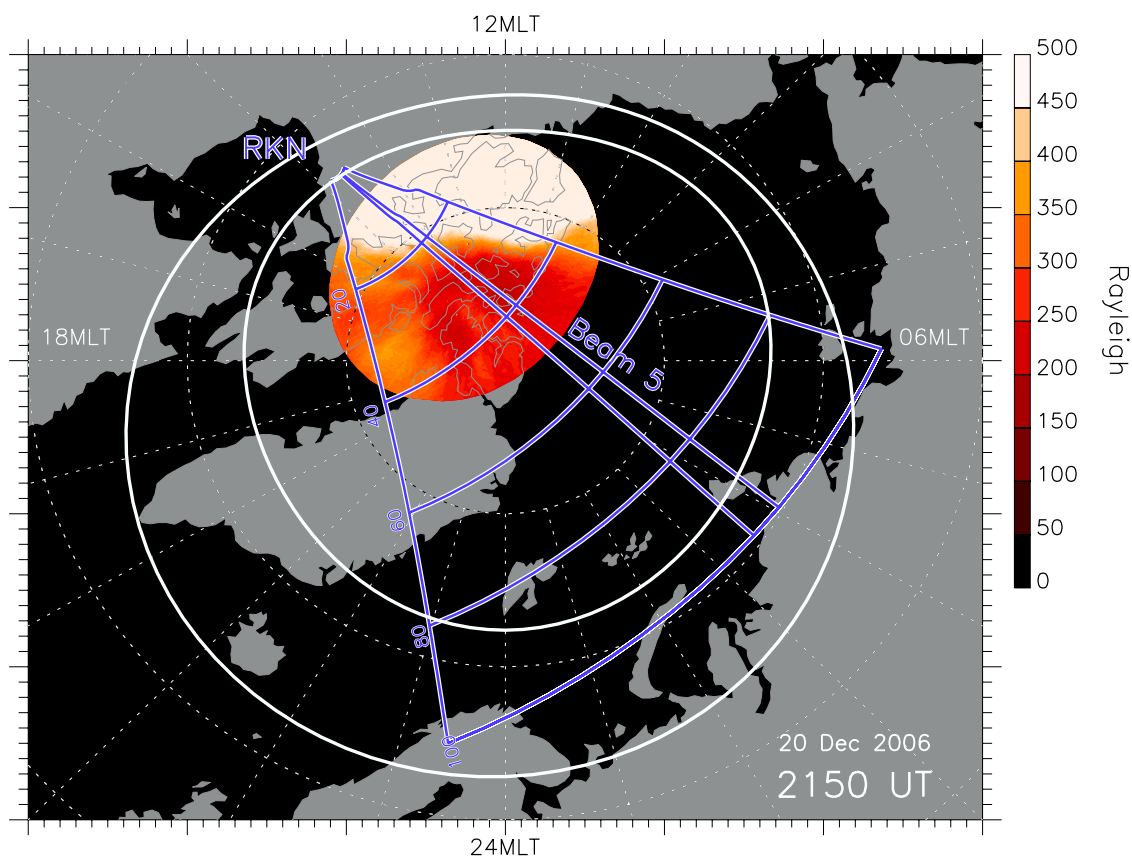


**Figure 1.** OI 630 nm airglow image recorded at 2150 UT on 20 December 2006. The image is shown in MLT/magnetic latitude coordinates, and the absolute airglow intensity is color-coded in units of Rayleigh. The FOV of the PolarDARN Rankin Inlet radar (blue lines) and the statistical location of the auroral oval (white lines) are superimposed. Range gates of 20, 40, 60, 80, and 100 are indicated within the FOV. Magnetic noon is to the top, and dotted circles represent magnetic latitudes of  $60^\circ$ ,  $70^\circ$ , and  $80^\circ$ .

that the spatial extent of radar patches (i.e., FAIs) was approximately 1000 km, which is almost comparable to that of polar patches itself. Since these past studies used the radar data only, the spatial relationship between electron density patches and accompanying FAIs has remained unclear.

[5] In the present study, two-dimensional coordinated simultaneous observations of polar cap patches were performed using an all-sky airglow imager at Resolute Bay and the newly constructed PolarDARN radar at Rankin Inlet, Canada. The data, obtained as OI 630 nm airglow images and decameter-scale FAIs determined by coherent HF radar, reveal the temporal evolution of the two-dimensional structures of both optical patches and FAIs. This allows us to directly compare spatial distributions of electron density patches and irregularities on the basis of a large number of simultaneous observations.

## 2. Instrumentation

[6] The all-sky airglow imager at Resolute Bay ( $74.73^\circ\text{N}$ ,  $265.07^\circ\text{E}$ ; AACGM latitude  $82.9^\circ$ ) has been in operation since January 2005 [Hosokawa *et al.*, 2006] as part of the Optical Mesosphere Thermosphere Imagers (OMTIs) [Shiokawa *et al.*, 1999]. The present analysis was conducted using airglow images obtained at a wavelength of 630.0 nm (OI, emission altitude of 200–300 km) taken every 2 min

with an exposure time of 30 s. The background continuum emission from the sky was sampled every 20 min at a wavelength of 572.5 nm, and was employed to derive the absolute intensity of the airglow lines [Shiokawa *et al.*, 2000].

[7] The PolarDARN Rankin Inlet radar ( $62.82^\circ\text{N}$ ,  $93.11^\circ\text{W}$ ; AACGM latitude  $72.96^\circ$ ), which forms part of the international SuperDARN network [Greenwald *et al.*, 1995; Chisham *et al.*, 2007], has been in operation since 2006. The radar has been used extensively to study various phenomena in the polar cap region, for which it has a favorable viewing geometry. On the day of the observations examined in this study, the radar was operating in the fast normal-scan mode. In the current version of this mode, the radar scans through 16 beams every minute, with an integration time of 3 s for each beam, which are binned into 100 range gates (the separation between the gates is 45 km). The operating frequency was stable between 12.2 and 12.5 MHz.

## 3. Observations

[8] The interval presented is 2100–2300 UT on 20 December 2006. Figure 1 shows a snapshot of the OI 630 nm airglow image at 2150 UT in MLT and magnetic latitude coordinates. The original all-sky images have been converted into altitude adjusted corrected geomagnetic (AACGM) coor-

dinates [Baker and Wing, 1989] assuming an emission height of 250 km. The field of view (FOV) of the Rankin Inlet radar has a large common volume with that of the all-sky imager at Resolute Bay, and Beam 5 of the Rankin Inlet radar covers the zenith of the all-sky imager. The statistical location of the auroral oval [Feldstein and Starkov, 1967] for the prevailing geomagnetic conditions during the interval under study ( $K_p = 3$ ) is also superimposed. The FOVs of these two instruments are well inside the polar cap boundary, and can be employed to visualize the dynamic behavior of polar cap patches.

[9] Almost half of the FOV of the all-sky imager is illuminated by the sun under the horizon, since the terminator at the  $F$  region height is substantially offset from the ground level terminator. The all-sky imager is also located very close to the noon meridian in the interval of interest. As patches are usually generated in the vicinity of the dayside cusp, the observational geometry considered allows us to visualize patches transported deep inside the polar cap along the streamline of antisunward plasma drift situated in the throat of the twin-cell convection pattern.

[10] Figures 2a and 2b show the IMF  $B_y$  and  $B_z$  as monitored by the ACE spacecraft located upstream of the Earth ( $X_{gsm} = 225.5 R_e$ ). A solar wind velocity of  $\approx 700 \text{ km s}^{-1}$  was measured by ACE, corresponding to a delay of 38 min between the observed IMF feature and incidence on the dayside magnetopause. An additional 2 min must be added to account for the propagation of Alfvén waves from the subsolar magnetopause to the dayside polar cap ionosphere. These calculations are based on the technique of Khan and Cowley [1999]. The time series of the IMF have been shifted accordingly. Except for a brief excursion to positive values between 2205 and 2230 UT, the IMF  $B_z$  component was predominantly negative in the observation period, representing favorable conditions for the generation of polar patches near the cusp and delivery into the central polar cap [Crowley, 1996]. The IMF  $B_y$  component was predominantly positive in the observation interval, although the sign switched many times. The positive skew of  $B_y$  may therefore add some dawn-to-dusk asymmetry to the antisunward convection in the central polar cap [Ruohoniemi and Greenwald, 1996, 2005; Ruohoniemi and Baker, 1998; Hosokawa et al., 2006].

[11] Figures 2c and 2d show the geographic south–north and east–west keograms of OI 630.0 nm airglow images. Four individual patches (A–D) are apparent as slanted traces of high airglow intensity moving from south to north and west to east. This southwest to northeast motion corresponds to antisunward motion slightly tilted toward dusk, consistent with the prevailing IMF conditions at the time of the observations. After the passage of patch D, which appeared at 2204 UT, no further patches appear within the FOV of the imager, probably owing to the effect of the northward IMF  $B_z$  interval (2205–2230 UT). Oksavik et al. [2006] demonstrated that patches can be formed owing to soft particle precipitation inside a lobe cell even during the northward IMF conditions. In such case, however, transportation of patches into the central polar cap is limited because sunward convection is dominant in the vicinity of the dayside cusp. Thus, patches are unlikely to appear at the latitude of Resolute Bay when the IMF  $B_z$  is directed positive.

[12] Figures 2e–2g show the Range-Time-Intensity (RTI) plots of backscatter power, line-of-sight Doppler velocity, and Doppler spectral width observed along beam 5 of the PolarDARN Rankin Inlet radar. As the polar patches pass through the zenith at Resolute Bay, the Rankin Inlet radar observes blobs of strong radar backscatter along beam 5, indicating that the optical patches have counterparts in the radar observation (i.e., FAIs). Interpretation of the line-of-sight Doppler velocities is difficult since beam 5 of the Rankin Inlet radar is oriented almost perpendicular to the direction of patch movement. However, the Doppler velocities within the blobs of FAIs are negative (away from the radar) during most of the interval presented, which is roughly consistent with the antisunward motion of the patches. We will discuss the relationship between the direction of motion of patches and the background ionospheric convection in the later part of this section by using the two-dimensional SuperDARN velocities derived with the map-potential technique [Ruohoniemi and Baker, 1998]. The spectral width within the blobs is narrow, less than  $100 \text{ m s}^{-1}$  at most times. Milan et al. [2002] reported that the spectral width within a patch starts high after inception, comparable with that of the cusp region, and subsequently decreases as the patch progresses to polar cap latitudes. The narrow spectral width observed within the central polar cap region for the present interval is therefore consistent with previous SuperDARN radar observations of polar cap patches [Milan et al., 2002; Oksavik et al., 2006].

[13] Figure 3 shows time sequences of OI 630.0 nm airglow images and the corresponding maps of radar backscatter power in the MLT/magnetic latitude coordinate system. The airglow images are picked at 10 min intervals between 2144 UT and 2234 UT, and the airglow distribution is shown as a percentage deviation from the 1 h running average. Polar patches are apparent in the images as cigar-shaped regions with significant positive deviation from the average luminosity. As the sequence progresses from 2144 UT, the patches move eastward from the dayside to the nightside until only patch D remains in the FOV. Patch D moves from the zenith of the all-sky imager at 2214 UT to the region close to the boresite of the radar at 2224 UT. At this time, the equatorward half of patch D is overwrapping the boresite of the radar FOV although the poleward half is slightly away from the boresite. Subsequently, patch D splits into two at 2234 UT.

[14] The backscatter power observed with the PolarDARN Rankin Inlet radar reveals three blobs of FAIs coincident with the three airglow patches at 2144 UT. The backscatter power depends on both the background noise level and the propagation (absorption along the ray path). Artificial blobs may occur if the signal absorption or background noise level varies. However, we have checked the background noise level during this interval and confirmed that the beams of weak backscatter are not due to extreme noise in those beam directions. It is interesting to note that the FAI blobs splits into two at 2224–2234 UT, as seen for patch D in the optical images. Another patch is formed westward of patch D at 2224/2234 UT. This newly-formed patch is seen more clearly in the radar data than in the optical data. This is because the dayside part of the FOV of the imager is illuminated by the sun under the horizon and optical patches sometimes become invisible. After the image at 2234 UT, the direction of plasma convection was suddenly changed to further duskward, and

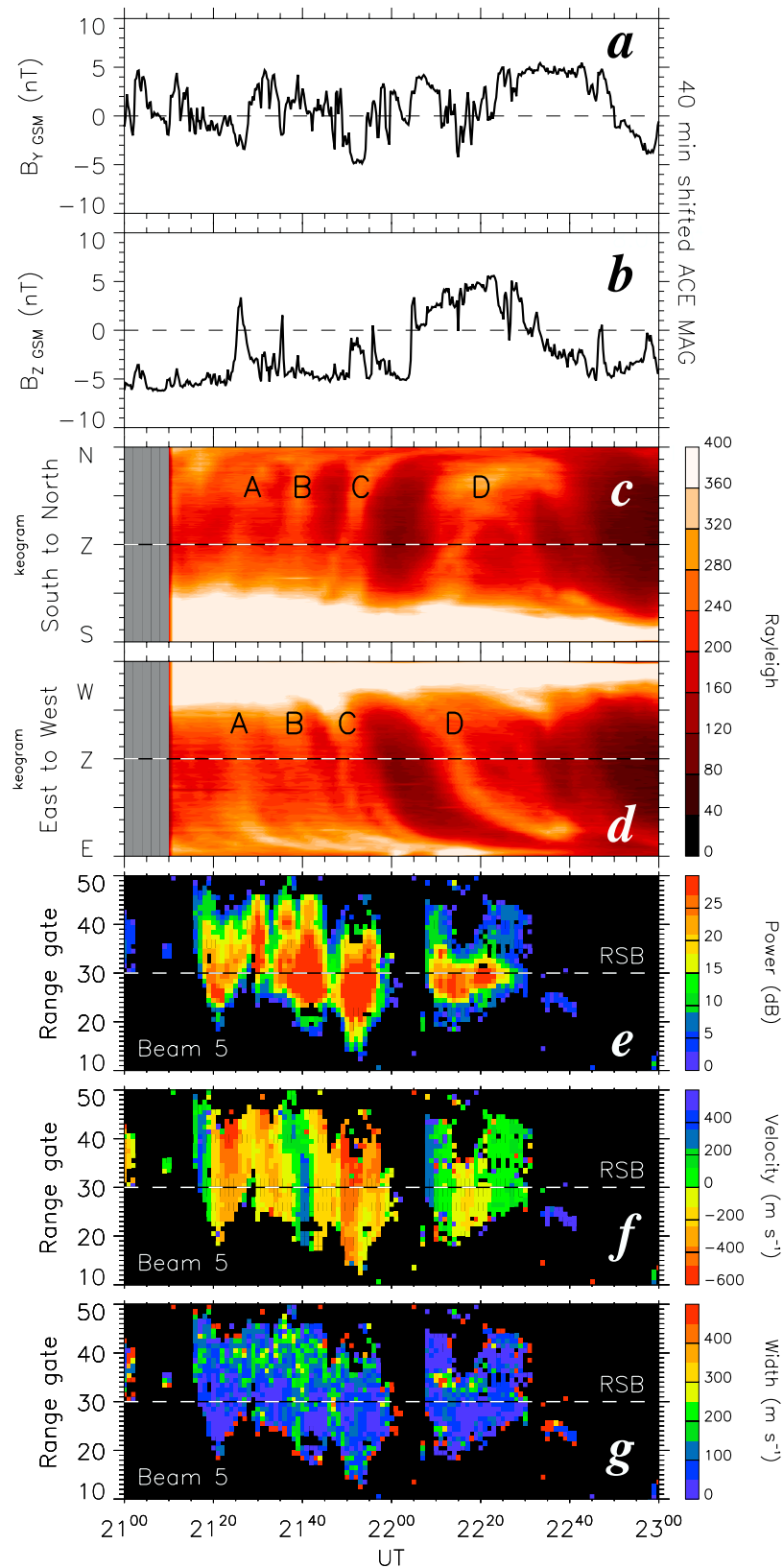


**Figure 2.** (a and b) IMF  $B_y$  and  $B_z$  components measured by the ACE spacecraft, time shifted by 40 min to allow for solar wind propagation delay. (c and d) North–south and east–west keograms of 630.0 nm all-sky images. (e–g) RTI plots of backscatter power, Doppler velocity, and Doppler spectral width from beam 5 of the Rankin Inlet radar. The vertical axis is range gate, separation between consecutive gates being 45 km. The horizontal dashed line indicates the zenith of the all-sky imager at Resolute Bay (range gate 30). Only backscatter from FAIs is shown (echoes regarded as ground scatter have been removed).

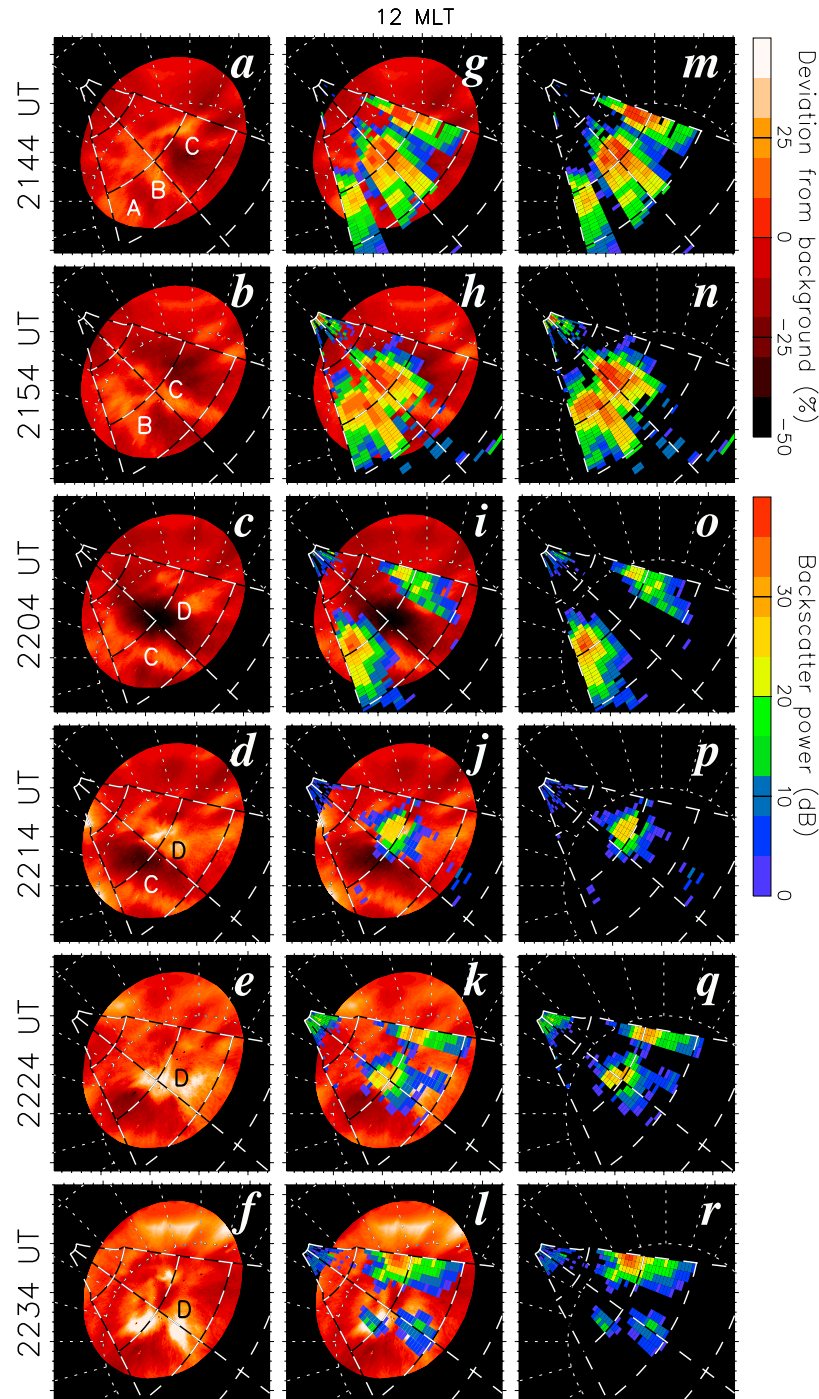


**Figure 3.** A sequence of (a–f) 630.0 nm airglow images and (m–r) radar backscatter power maps at 10 min intervals from 2144 UT. (g–l) Superposition of airglow and radar backscatter. The airglow images show deviation from 1 h running averages indicating weak perturbations in airglow intensity associated with patches. The FOV of the Rankin Inlet radar is indicated by dashed lines.

this newly formed patch got out of the FOV of the radar and imager.

[15] The one-to-one spatial collocation between polar patches in the optical image and the blobs of FAIs in the radar observations is generally good. This apparent correspondence between optical patches and radar FAIs can be identified not only in the time frames shown in Figure 3 but also throughout the interval of interest. An animation show-

ing the evolution of the optical patches and radar backscatter at a rate of one frame every 2 min accompanies the electronic version of this article (see Animation S1).<sup>1</sup> The spatial structures of optical patches and radar FAIs are thus coincident and move almost in tandem in the antisunward direction.

<sup>1</sup>Auxiliary materials are available in the HTML. doi:10.1029/2008JA013707.

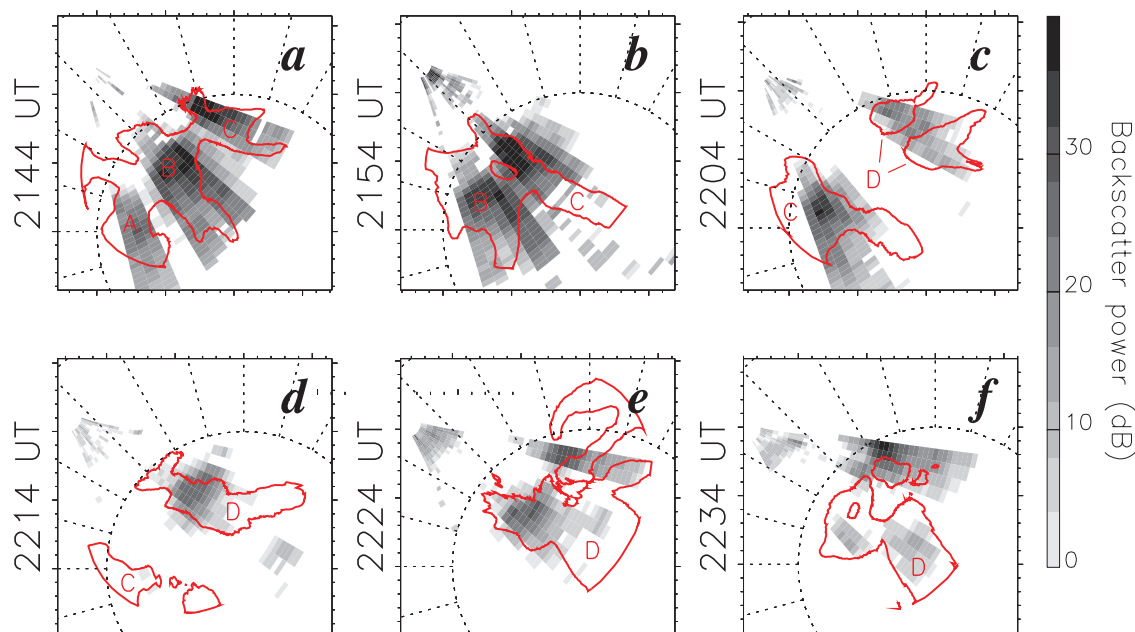


**Figure 4.** A detailed comparison of airglow patches and radar FAIs at 10 min intervals from 2144 UT. The boundary of airglow patches is defined as a contour of airglow intensity 10% brighter than the 1 h running average (red line). The radar backscatter power is overplotted in grey scale.

[16] To see the spatial collocation between optical patches and radar FAIs in more detail, it is necessary to define boundaries of the airglow patches. A definition of polar patches suggested by Crowley [1996] is that the electron density within the patch is two or more times denser than the background level. We need a definition in terms of airglow intensity. OI 630 nm airglow intensity obtained with the ground-based all-sky imager is known to be proportional to the electron density at 250–300 km altitudes in the  $F$  region [Barbier, 1959; Barbier and Glaume, 1962]. However, the quantitative relationship between electron density and airglow intensity is not so simple. Here, we define the boundary of airglow patches as a contour of airglow intensity 10% brighter than the 1 h running average (note that “1 h running average” does not correspond to the background level). Using this definition, the boundaries of outstanding airglow patches (patches A–D) are presented in Figure 4 as red contours, where radar backscatter power is overplotted in grey scale.

[17] As seen in Figure 4, the overall collocation of optical and radar patches is remarkable once we take the difference between the spatial resolution of the optical and radar observations into account. In particular we observe that the radar echoes are distributed not only on the trailing edge but also almost on the entire part of optical patches. However, the area of an optical patch is sometimes larger than that of a radar’s FAIs (Patch C in Figures 4b and 4c and Patch D in Figures 4d and 4e). Note that this kind of mismatch occurs mostly in distant radar ranges. We will discuss this point in more detail in the later part of this paper.

[18] As mentioned in the previous part, the line of sight of the radar beams from Rankin Inlet is almost perpendicular to the moving direction of patches as inferred from the optical observation. This makes it difficult to examine the relationship between patch motion and background plasma

convection only from the line-of-sight Doppler velocity data. Figure 5a shows the OI 630 nm optical image at 2158 UT. Superimposed contours give a pattern of the high-latitude electrostatic potential derived with the map-potential technique [Ruohoniemi and Baker, 1998]. The streamline of the polar cap convection pattern over Resolute Bay is slightly tilted toward dusk, which is consistent with the moving direction of the optical patches. This confirms that polar cap patches are transported along the streamline of the polar cap plasma convection.

[19] Here, we try to find the possible source of the patches by using the data from a SuperDARN radar at auroral latitudes. Figure 5b shows a snapshot of the Doppler velocity data at 2158 UT as obtained by the SuperDARN Prince George radar ( $53.98^{\circ}\text{N}$ ,  $122.59^{\circ}\text{W}$ ), in which the backscatter power data from the Rankin Inlet radar are overplotted. At this time, the Rankin Inlet radar observed Patch B and C drifting across the FOV. As shown in Figure 4b, these patches were also detected by the all-sky imager at Resolute Bay. On the dayside, the Prince George radar observed fast antisunward plasma flow of  $1500\text{ m s}^{-1}$  at around  $72^{\circ}$  magnetic latitude (shown as a rectangle). Comparing the location of this fast flow with the convection pattern shown in Figure 5a, the convection throat was located in the vicinity of the enhanced antisunward flow region.

[20] Figure 6b shows the temporal variations of the Doppler velocity along beam 9 of Prince George. A backscatter region with Doppler velocity directed away from the radar, which corresponds to antisunward convection, appeared 5 min before 2100 UT and were observed for about 75 min. This enhanced convection is possibly associated with an enhanced equatorial magnetopause reconnection during southward IMF conditions, which is consistent with the fact that the antisunward flow suddenly disappeared when the IMF  $B_z$  (shown in Figure 6a) turned to positive at around

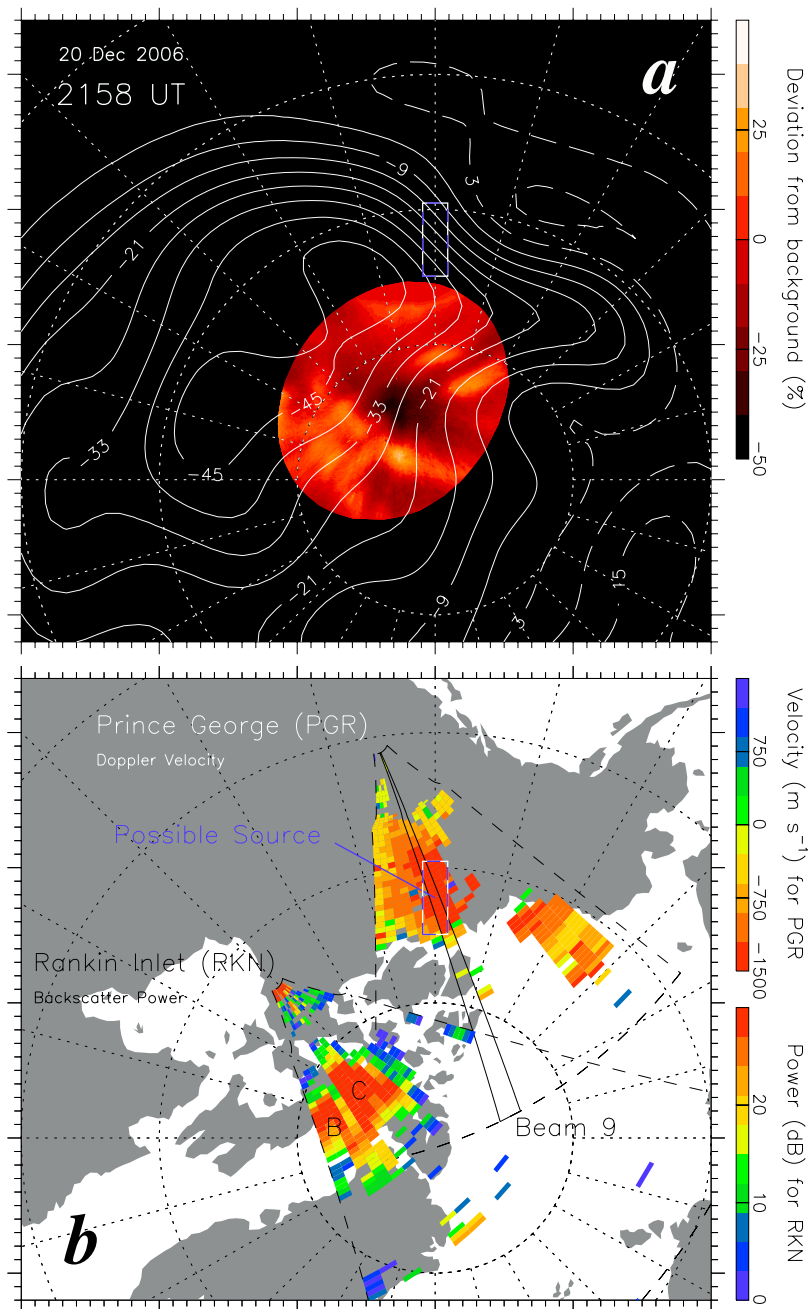


**Figure 5.** (a) OI 630 nm airglow image at 2158 UT. Superimposed contours give a pattern of the high-latitude electrostatic potential derived with the map-potential technique [Ruohoniemi and Baker, 1998]. (b) A snapshot of the Doppler velocity data from the Prince George radar and the backscatter power data from the Rankin Inlet radar at 2158 UT.

2205 UT. It is interesting to note that there exist some temporal variations of the Doppler velocities within this echo region. Past studies suggested that patches could be formed through temporal changes in the convection pattern under the influence of variations in the IMF and the magnetopause reconnection rate [e.g., Decker et al., 1994; Lockwood and Carlson, 1992]. Especially a time-varying antisunward convection could act as a primary generation mechanism of patches. Thus, this region of time-varying antisunward convection at around  $72^\circ$  magnetic latitude is likely to be the possible source of the patches seen over Resolute Bay. Figure 6d shows the RTI plot of the backscatter power from beam 5

of Rankin Inlet. Polar cap patches were observed for 75 min from 2115 UT to 2230 UT. This duration is very similar to that of the antisunward flow region detected by Prince George. This correspondence also suggests that the antisunward flow region observed by the Prince George radar is associated with a formation of patches observed with the Rankin Inlet radar.

[21] If the antisunward flow region observed with Prince George is the source of the patches, early formative behavior of patches should be observed in the backscatter power data shown in Figure 6c. However, in the poleward part of the backscatter region we find no clear signature of poleward moving blobs of FAIs, which is known as a manifestation of

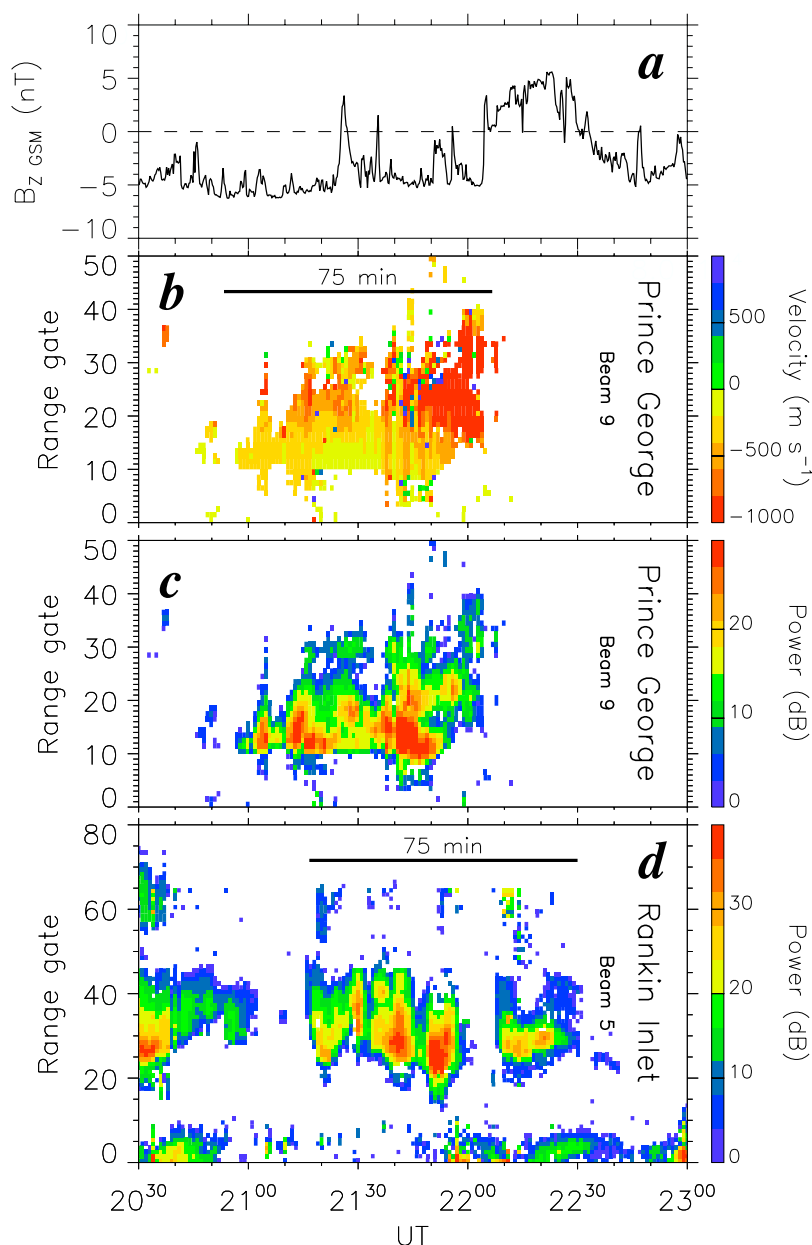


**Figure 6.** (a) IMF  $B_z$  components measured by the ACE spacecraft time shifted by 40 min to allow for the solar wind propagation delay. RTI plots of the (b) Doppler velocity and (c) backscatter power from beam 9 of the Prince George radar. (d) Backscatter power data from beam 5 of the Rankin Inlet radar in RTI format.

early formative behavior of patches [e.g., Milan *et al.*, 2002]. During the interval of interest, two other SuperDARN radars (Saskatoon and Kodiak) were looking at the dayside part of the twin-cell convection pattern. However, these two radars also did not show any signature of poleward moving blobs of irregularities. This is probably because propagation was not appropriate for the radar to observe patches appearing in distant range gates. Hence, we cannot track the patches from their origin in the convection throat and all the way to Resolute Bay.

#### 4. Discussion

[22] Radar backscatter and the 630 nm airglow enhancement associated with polar patches were simultaneously

observed using the all-sky airglow imager at Resolute Bay and the PolarDARN Rankin Inlet radar. A comparison of the spatial distributions of radar backscatter and airglow enhancement for the observation interval on 20 December 2006 revealed the presence of decameter-scale FAIs almost within the entire airglow-enhanced region.

[23] Prior to discussing the correlation between the observed polar patches and FAI blobs, it is necessary to consider the accuracy of the backscatter location determined by the SuperDARN radar. Backscatter echoes are detected by a coherent HF radar when conditions satisfy two critical requirements: FAIs must be present within the FOV, and the ionospheric propagation must be such that HF waves can reach the ionosphere at a substantial distance from the radar site. In the examples shown here, the propagation condition

does not appear to be a limiting factor at the radar ranges relatively close to the radar site (say <1200 km). However, Figure 4 shows that airglow patches and radar FAIs are sometimes not collocated at the distant radar ranges.

[24] *Yeoman et al.* [2001] estimated the potential error of the standard algorithm employed by the SuperDARN to determine the location of backscatter based on simultaneous observations by the SuperDARN Finland radar and the EISCAT Tromsø heating facility. The accuracy of echo location for half-hop ionospheric backscatter in that case was found to be 15 km or less. In the current observations, the ground range in which patch-associated backscatter echoes appeared is 1000–1500 km, which corresponds to half-hop ionospheric scatter. As the structures considered in the present study are large, up to 500 km in horizontal extent, the error of  $\approx 15$  km can be ignored in a discussion of the spatial relationship between optical patches and radar irregularities.

[25] Electron density irregularities associated with polar cap patches have been observed throughout the polar cap region [e.g., *Weber et al.*, 1984]. The irregularities are often more intense on the trailing edge than on the leading edge [*Weber et al.*, 1984], implying that the generation mechanism is GDI. By applying a quantitative patch definition for spacecraft measurements [*Coley and Heelis*, 1995], *Kivanc and Heelis* [1997] identified four groups of patches on the basis of structural characteristics: fully structured patches, patches with structure only on the edges, patches with only one structured edge, and unstructured patches. It was demonstrated that the majority of patches belong to the first two categories.

[26] On the basis of an examination of nighttime FAIs possibly associated with polar patches, *Ogawa et al.* [1998] suggested that the spatial scale of these FAIs should be comparable to that of the patch itself. This implies that patches observed on the nightside in that case were fully structured. By contrast, *Milan et al.* [2002] reported stronger backscatter power on the trailing edge of radar patches observed by the SuperDARN Finland radar in the vicinity of the dayside cusp, implying that patches near the cusp region are structured only on the trailing edge. The findings of these two past studies suggest that the irregularities associated with patches are distributed only on the trailing edge shortly after generation near the cusp, after which FAIs prevail over the entire region of the patch as the patch travels across the polar cap.

[27] The present observations demonstrate that the FAIs are already distributed over the entire region of the optical patch when the patch enters the FOV of the all-sky imager and the Rankin Inlet radar. This suggests that most of the patches appeared to be almost fully structured (matured) upon entry into the FOV of the radar. Of course, not all patches would be fully structured in the sense that radar echoes did not always fill the patches. In particular, there exist some occasions in which the backscatter power seems to be higher at the trailing edge of the optical patches (in Figure 2g for example) although radar echoes are distributed over almost the entire part of the optical patches. This may indicate that structuring process is still working and some of the patches are not matured completely. However, we cannot find any systematic difference in the radar backscatter power at the leading and trailing edges of the patches. Thus, in the following discus-

sion, we deem that structuring of the patches is “almost” completed when they enter into the FOV of the radar.

[28] Here, we try to estimate how long it did take for the patches to be almost fully structured. As shown in Figure 5b, the possible source of the patches seen over Resolute Bay was at around  $72^\circ$  magnetic latitude. If we assume that all of the patches observed at Resolute Bay were formed around this latitude, the distance from the source to the zenith of Resolute Bay along the streamline of the convection shown in Figure 5a is approximately 1500–1800 km. It is not so easy to derive the velocity of traveling patches because the velocity of patches would change as they travel from the source to the central polar cap area. The velocity of patches near the source can be estimated to be  $1500 \text{ m s}^{-1}$  from the line-of-sight Doppler velocity obtained by the Prince George radar. In the central polar cap area, however, the line-of-sight Doppler velocity from the Rankin Inlet radar cannot be used because the direction of patch motion is almost perpendicular to the radar beam direction. Then, we calculated the time it took for the patches to traverse the radar beams of the Rankin Inlet radar and estimated the velocity of the patches. As shown in Figure 3, patch C appeared in the westernmost beam of the radar at around 2144 UT and disappear in the easternmost beam at around 2204 UT. It took approximately 20 min to traverse the radar beams in azimuthal direction. The length of the travel path of patch C across the FOV is about 1500 km. Thus, possible moving speed of the patch is estimated to be  $1200 \text{ m s}^{-1}$ , which is slightly less than the speed estimated from the data of Prince George ( $1500 \text{ m s}^{-1}$ ). However, this is reasonable because the convection speed in the central polar cap area is generally smaller than that in the vicinity of the convection throat. If we employ the average of these two velocities  $\approx 1350 \text{ m s}^{-1}$  as an average propagation speed of the patches, it takes only approximately 20–25 min for patches to travel from their source to the zenith of Resolute Bay. If we take a closer look at Figures 6b and 6c, the Rankin Inlet radar started observing the patches about 20–25 min after the onset of the antisunward flow detected with the Prince George radar. This confirms that the estimated travel time of 20–25 min is reasonable. The current estimation indicates that the structuring process is almost completed within 20–25 min after initiation.

[29] *Moen et al.* [2002] reported a good collocation between the FAIs in the cusp region and 630 nm auroral precipitation. In addition, they employed radio tomographic images of electron density in the vicinity of the cusp radar echoes and claimed the rapid growth of radar backscatter could not be explained only by the gradient drift instability process. They proposed that the initial source of the decameter-scale features responsible for the irregularities may result from fine scale structure within the precipitation itself.

[30] In a series of papers by *Gondarenko and Guzdar* [*Gondarenko and Guzdar*, 2004, and references therein] three-dimensional nonlinear simulations of polar cap patches were performed in an attempt to model the generation of mesoscale structures within a patch. It was demonstrated that the primary structuring occurred on the trailing edge of the patches to produce long elongated fingers oriented perpendicular to the ambient electron density contour and magnetic field. The formation of such finger-like structures can be attributed to the linear development of GDI. However, the highly elongated fingers are unstable to a secondary

Kelvin-Helmholtz instability, which breaks the structures into smaller-scale vortices. Although the initial instability develops only on the trailing edge, the irregularities do not remain localized on the edges of the patches and eventually permeate through the entire patch. Simulations suggest a time scale of approximately 1 h for the patch to become fully structured. However, the present observations indicate that the structuring process may be substantially faster, since the patches appear to be almost fully structured upon entry into the FOV under study. A more rapid structuring process may therefore be required in order to explain the present observations.

[31] In the simulations of *Gondarenko and Guzdar* [2004, and references therein], patches are infinite in the direction perpendicular to the background convection. Then, primary GDI seems to occur only on the trailing edge of the patches. In reality, however, patches are finite in all directions. *Keskinen and Ossakow* [1982] analytically demonstrated that electron density structure is unstable at any part of its boundary except where the background drift and the density gradients are completely antiparallel to one another. This suggests that the primary structuring process can occur at any edges of patches except for a small region near the leading edge. In other words, elongated fingers can be produced at almost all edges of patches, which could make the structuring process much faster.

[32] The other important point to note is that patches are not always homogeneous near the cusp at the time of their generation. It is well known that the cusp is full of 10–100 km structures caused by inhomogeneous soft particle precipitations and time-varying turbulent electric field [*Oksavik et al.*, 2004a, 2004b, 2005]. If we already have 10–100 km structures within patches, it does not take a long time for GDI to break these 10–100 km structures into irregularities of decameter scale. This may then also contribute to the rapid structuring of patches observed in the present study.

[33] *Gondarenko et al.* [2003] suggested that since the GDI depends on the magnitude and direction of the background flow velocity, the evolution of mesoscale structures associated with patches will be strongly affected by the temporal variability of ionospheric flow velocities. If the flow velocity changes in direction, the structuring process initiated on the trailing edge of the patch will develop on the leading edge, and the instability can eventually progress into the bulk of the patch. During the interval of interest, the IMF  $B_y$  switched sign frequently, which could indicate changes in the direction of cusp plasma flow. This occasional change in the direction of convection may have contributed to the rapid structuring of patches inferred from the present observations.

## 5. Conclusion

[34] Polar cap patches passing over Resolute Bay were detected optically with an all-sky airglow imager at Resolute Bay using enhanced brightness in the OI 630.0 nm emissions while the polar cap was in darkness. The patches had horizontal scales ranging between 500 and 1000 km. In coordinated HF radar measurements made with the PolarDARN radar at Rankin Inlet, we have found that the radar echoes from the patches had a narrow spectral width and that the radar echoes were produced over the entire area of the airglow enhancement of the polar patches. The spectral width

and distribution of echoes throughout the patches both indicated that the patches had reached a mature stage in their evolution which meant that they were almost fully structured by the time they appeared in the field of view of the all-sky imager. While the full structuring of “mature” patches has been predicted by numerical simulations, we have noticed, on the basis of the speed of the patches and their distance to the cusp, that the time scale needed to reach maturity had to be of the order of 20–25 min or less, which implies that the structuring was taking place more rapidly than expected for the event studied here.

[35] We also noticed that not all patches would be fully structured in the sense that radar echoes did not always fill the patches. In particular, when a patch broke into two, the radar power decreased in each patch while only one of the sub-patches ended being fully structured. We have left an investigation of origin of this dynamic change in the relationship between optical patches and the radar irregularities to a future paper, since the changes are complex and appear to be related to changes in the convection pattern. Studies of a more statistical nature also had to be left to future work since they involve the development of automated detection algorithms that have yet to be perfected.

[36] **Acknowledgments.** The authors thank Y. Katoh, M. Satoh, and T. Katoh of the Solar-Terrestrial Environment Laboratory (STEL), Nagoya University, for kind support in airglow imaging observations. This work was supported by a Grant-in-Aid for Scientific Research (19403010) from the Ministry of Education, Culture, Sports, Science and Technology of Japan and by Project 2 of the Geospace Research Center, STEL. The PolarDARN Rankin Inlet radar was constructed using funds from the Canada Foundation for Innovation, Saskatchewan Learning, and the Canadian Space Agency (CSA) and is operated using funds from a CSA contract and an NSERC Canada Major Facilities Access grant. The optical observation at Resolute Bay was supported by NSF cooperative agreement ATM-0608577. The authors also wish to thank N. Ness at the Bartol Research Institute for access to data from MFI and SWE instruments on board the ACE spacecraft. Special thanks are extended to staff of the Narwhal Arctic Service at Resolute Bay for kind and helpful support in operating the optical instrument.

[37] Zuyin Pu thanks Kjellmar Oksavik and another reviewer for their assistance in evaluating this paper.

## References

- Baker, K. B., and S. Wing (1989), A new magnetic coordinate system for conjugate studies of high latitudes, *J. Geophys. Res.*, *94*, 9139.
- Barbier, D. (1959), Recherches sur la raie 6300 de la luminescence atmosphérique nocturne, *Ann. Geophys.*, *15*, 179–217.
- Barbier, D., and J. Glaume (1962), La couche ionosphérique nocturne F dans la zone intertropicale et ses relations avec l’mission de la raie 6300 du ciel nocturne, *Planet. Space Sci.*, *9*, 133–149.
- Basu, S., Su. Basu, P. K. Chaturvedi, and C. M. Bryant Jr. (1994), Irregularity structures in the cusp/left and polar cap regions, *Radio Sci.*, *29*, 195.
- Chisham, G., et al. (2007), A decade of the Super Dual Auroral Radar Network (SuperDARN): scientific achievements, new techniques and future directions, *Surv. Geophys.*, *28*, 33–109, doi:10.1007/s10712-007-9017-8.
- Coley, W. R., and R. A. Heelis (1995), Adaptive identification and characterization of polar ionization patches, *J. Geophys. Res.*, *100*, 23,819.
- Crowley, G. (1996), Critical review of ionospheric patches and blobs, in *Review of Radio Science 1993–1996*, edited by W. R. Stone, p. 619, Oxford Univ. Press, New York.
- Decker, D., C. Valladares, R. Sheehan, S. Basu, D. Anderson, and R. Heelis (1994), Modeling daytime F layer patches over Sondrestrom, *Radio Sci.*, *29*, 249.
- Feldstein, Y. I., and G. V. Starkov (1967), Dynamics of auroral belt and polar geomagnetic disturbance, *Planet. Space Sci.*, *15*, 209.
- Gondarenko, N. A., and P. N. Guzdar (2004), Plasma patch structuring by the nonlinear evolution of the gradient drift instability in the high-latitude ionosphere, *J. Geophys. Res.*, *109*, A09301, doi:10.1029/2004JA010504.
- Gondarenko, N. A., P. N. Guzdar, J. J. Sojka, and M. David (2003), Structuring of high latitude plasma patches with variable drive, *Geophys. Res. Lett.*, *30*(4), 1165, doi:10.1029/2002GL016437.

- Greenwald, R. A., et al. (1995), DARN/SuperDARN: A global view of the dynamics of high-latitude convection, *Space Sci. Rev.*, *71*, 761.
- Hosokawa, K., K. Shiokawa, Y. Otsuka, A. Nakajima, T. Ogawa, and J. D. Kelly (2006), Estimating drift velocity of polar cap patches with all-sky airglow imager at Resolute Bay, Canada, *Geophys. Res. Lett.*, *33*, L15111, doi:10.1029/2006GL026916.
- Keskinen, M. J., and S. L. Ossakow (1982), Nonlinear evolution of plasma enhancements in the auroral ionosphere. I. Long wavelength irregularities, *J. Geophys. Res.*, *87*, 144.
- Khan, H., and S. W. H. Cowley (1999), Observations of the response time of high-latitude ionospheric convection to variations in the interplanetary magnetic field using EISCAT and IMP-8 data, *Ann. Geophys.*, *17*, 1306.
- Kivanc, O., and R. A. Heelis (1997), Structures in ionospheric number density and velocity associated with polar cap ionization patches, *J. Geophys. Res.*, *102*, 307.
- Lockwood, M., and H. C. Carlson Jr. (1992), Production of polar cap electron density patches by transient magnetopause reconnection, *Geophys. Res. Lett.*, *19*, 1731.
- MacDougall, J., and P. T. Jayachandran (2007), Polar patches: Auroral zone precipitation effects, *J. Geophys. Res.*, *112*, A05312, doi:10.1029/2006JA011930.
- Milan, S. E., M. Lester, and T. K. Yeoman (2002), HF radar polar patch formation revisited: summer and winter variations in dayside plasma structuring, *Ann. Geophys.*, *20*, 487.
- Milan, S. E., S. Basu, T. K. Yeoman, and R. E. Sheehan (2005), A comparison of satellite scintillation measurements with HF radar backscatter characteristics, *Ann. Geophys.*, *23*, 3451–3455.
- Moen, J., I. K. Walker, L. Kersley, and S. E. Milan (2002), On the generation of cusp HF backscatter irregularities, *J. Geophys. Res.*, *107*(A4), 1044, doi:10.1029/2001JA000111.
- Ogawa, T., N. Nishitani, M. Pinnock, N. Sato, H. Yamagishi, and A. S. Yukimatu (1998), Antarctic HF radar observations of irregularities associated with polar patches and auroral blobs: A case study, *J. Geophys. Res.*, *103*, 26,547.
- Oksavik, K., F. Soraas, J. Moen, R. Pfaff, J. A. Davies, and M. Lester (2004a), Simultaneous optical, CUTLASS HF radar, and FAST spacecraft observations: Signatures of boundary layer processes in the cusp, *Ann. Geophys.*, *22*, 511–525.
- Oksavik, K., J. Moen, and H. C. Carlson (2004b), High-resolution observations of the small-scale flow pattern associated with a poleward moving auroral form in the cusp, *Geophys. Res. Lett.*, *31*, L11807, doi:10.1029/2004GL019838.
- Oksavik, K., J. Moen, H. C. Carlson, R. A. Greenwald, S. E. Milan, M. Lester, W. F. Denig, and R. J. Barnes (2005), Multi-instrument mapping of the small-scale flow dynamics related to a cusp auroral transient, *Ann. Geophys.*, *23*, 2657.
- Oksavik, K., J. M. Ruohoniemi, R. A. Greenwald, J. B. H. Baker, J. Moen, H. C. Carlson, T. K. Yeoman, and M. Lester (2006), Observations of isolated polar cap patches by the European Incoherent Scatter (EISCAT) Svalbard and Super Dual Auroral Radar Network (SuperDARN) Finland radars, *J. Geophys. Res.*, *111*, A05310, doi:10.1029/2005JA011400.
- Pedersen, T., B. Fejer, R. Doe, and E. Weber (1998), Incoherent scatter radar observations of horizontal F region plasma structure over Sondrestrom, Greenland, during polar cap patch events, *Radio Sci.*, *33*, 1847.
- Pedersen, T., B. Fejer, R. Doe, and E. Weber (2000), An incoherent scatter radar technique for determining two-dimensional horizontal ionization structure in polar cap F region patches, *J. Geophys. Res.*, *105*, 10,637.
- Rodger, A. S., M. Pinnock, J. R. Dudeney, K. B. Baker, and R. A. Greenwald (1994), A new mechanism for polar patch formation, *J. Geophys. Res.*, *99*, 6425.
- Ruohoniemi, J. M., and K. B. Baker (1998), Response of high latitude convection to a sudden southward IMF turning, *Geophys. Res. Lett.*, *25*, 2913.
- Ruohoniemi, J. M., and R. A. Greenwald (1996), Statistical patterns of high-latitude convection obtained from Goose Bay HF radar observations, *J. Geophys. Res.*, *101*, 21,743.
- Ruohoniemi, J. M., and R. A. Greenwald (2005), Dependencies of high-latitude plasma convection: Consideration of interplanetary magnetic field, seasonal, and universal time factors in statistical patterns, *J. Geophys. Res.*, *110*, A09204, doi:10.1029/2004JA010815.
- Shiokawa, K., Y. Katoh, M. Satoh, M. K. Ejiri, T. Ogawa, T. Nakamura, T. Tsuda, and R. H. Wiens (1999), Development of optical mesosphere thermosphere imagers (OMTI), *Earth Planets Space*, *51*, 887.
- Shiokawa, K., Y. Katoh, M. Satoh, M. K. Ejiri, and T. Ogawa (2000), Integrating-sphere calibration of all-sky cameras for nightglow measurements, *Adv. Space Res.*, *26*, 1025.
- Weber, E. J., J. Buchau, J. G. Moore, J. R. Sharber, R. C. Livingston, J. D. Winningham, and B. W. Reinisch (1984), F layer ionization patches in the polar caps, *J. Geophys. Res.*, *89*, 1683.
- Weber, E. J., et al. (1986), Polar cap F patches: Structure and dynamics, *J. Geophys. Res.*, *91*, 12,121.
- Yeoman, T. K., D. M. Wright, A. J. Stocker, and T. B. Jones (2001), An evaluation of range accuracy in the Super Dual Auroral Radar Network over-the-horizon HF radar systems, *Radio Sci.*, *36*, 801.

---

D. A. Andre, G. J. Sofko, and J.-P. St-Maurice, Institute for Space and Atmospheric Studies, Department of Physics and Engineering Physics, University of Saskatchewan, 116 Science Place, Saskatoon, SK S7N 5E2, Canada. (dieter.andre@usask.ca; George.Sofko@usask.ca; jp.stmaurice@usask.ca)

K. Hosokawa, Department of Information and Communication Engineering, University of Electro-Communications, Chofugaoka 1-5-1, Chofu, Tokyo 182-8585, Japan. (hosokawa@ice.ucc.ac.jp)

T. Ogawa, National Institute of Information and Communications Technology, Nukui-Kitamachi 4-2-1, Koganei, Tokyo 184-8795, Japan. (taogawa@nict.go.jp)

Y. Otsuka and K. Shiokawa, Solar-Terrestrial Environment Laboratory, Nagoya University, Furo-cho, Chikusa-ku, Nagoya Aichi 464-8601, Japan. (otsuka@stelab.nagoya-u.ac.jp; shiokawa@stelab.nagoya-u.ac.jp)